

Precise Centre National d'Etudes Spatiales orbits for TOPEX/POSEIDON: Is reaching 2 cm still a challenge?

F. Nouël, J. P. Berthias, M. Deleuze, A. Guitart, P. Laudet, A. Piuze, D. Pradines, and C. Valorge

Centre National d'Etudes Spatiales, Toulouse, France

C. Dejoie and M. F. Susini

Compagnie Internationale de Services Informatiques, Toulouse, France

D. Taburiau

Cap Sesa Région, Toulouse, France

Abstract. To achieve maximum benefit from the altimetric data collected by the French-American TOPEX/POSEIDON spacecraft, radial orbit accuracy of 10 cm or better is required. This unprecedented requirement led the French Space Agency Centre National d'Etudes Spatiales (CNES) to develop a new high-accuracy tracking system, Doppler orbitography and radiopositioning integrated by satellite (DORIS), and a new precision orbit production facility, the Service d'Orbitographie DORIS. A global effort produced new models and new orbit determination strategies. The result of these efforts has been assessed after 1 year of operation. The original goal has clearly been met, and the TOPEX/POSEIDON orbits produced by NASA and CNES agree to better than the 5 cm RMS level in the radial direction. At this level of accuracy, traditional techniques cannot correctly describe the actual orbit error, and some new procedures are proposed.

1. Introduction

In order to monitor climatologically sensitive signals in the ocean's topography from radar altimetric measurements, the orbit of the satellite carrying the payload must be known with an accuracy of the order of 10 cm. While this represented an abstract goal, it was adopted for the French-American TOPEX/POSEIDON (T/P) mission. To deal with the orbit problem, the efforts on the French side were concentrated on two aspects, namely, developing a tracking system, Doppler orbitography and radiopositioning integrated by satellite (DORIS), able to accurately determine the location of the satellite and designing an orbit determination system to handle these data and provide the satellite position on a timely basis to the oceanographic community.

The Centre National d'Etudes Spatiales (CNES) prepared for the T/P precise orbit determination task in collaboration with the Space Geodesy Branch of the Goddard Space Flight Center (GSFC) and the Center for Space Research (CSR) of the University of Texas. Besides an excellent relationship motivated by the will to succeed, and a scrupulous desire for rigorous comparison, there were also significant individual differences in the strategies to compute orbits among centers. These are worth describing and bring additional confidence in the results, especially when centimeters of accuracy is the result. While there is no absolute way to certify to the users that the 10-cm accuracy is obtained, an effective strategy is to produce several orbits with different software

or procedures and compare them. As a result, there are two official orbits which are included in the altimeter geophysical data record (GDR): the CNES precise orbit ephemeris (CNES POE) and the NASA POE provided by the Service d'Orbitographie DORIS (SOD) and the GSFC, respectively. The SOD strategies and the cross-checking procedures will be examined with an emphasis on what is different and unique to the SOD processing procedures.

The adjustment of the DORIS measurement model parameters is explained, along with the procedures used to check the accuracy of the observations which are processed to compute the orbit. This information is also provided to other users.

The original 10-cm goal has been certainly surpassed as demonstrated by the results seen after 1 year of T/P activity. This is also confirmed by the experimental Global Positioning System (GPS) tracking system associated with the proposed "reduced dynamics" technique [Bertiger *et al.*, this issue]. As an external check, this experiment is very interesting since it tests the accuracy of the orbit which is provided to the oceanographers. This was possible on some entire, or part of, T/P 10-day ground track repeat cycles. Moreover, as time went by, during the first year of T/P's life, the experiment grew in maturity and by solving for an unexplained 6-cm bias (at least to our knowledge) gave results closer to the GDR orbits. Generally, comparisons will be made between CNES POE and NASA POE as part of the production procedures, and the results will cover any T/P cycle unless otherwise specified.

The present SOD estimate of the radial RMS error is about 2.5 cm (RMS over 10 days). It is necessary, when reaching the 1-inch (2.54 cm) level, to better understand what is

Copyright 1994 by the American Geophysical Union.

Paper number 94JC01039.
0148-0227/94/94JC-01039\$05.00

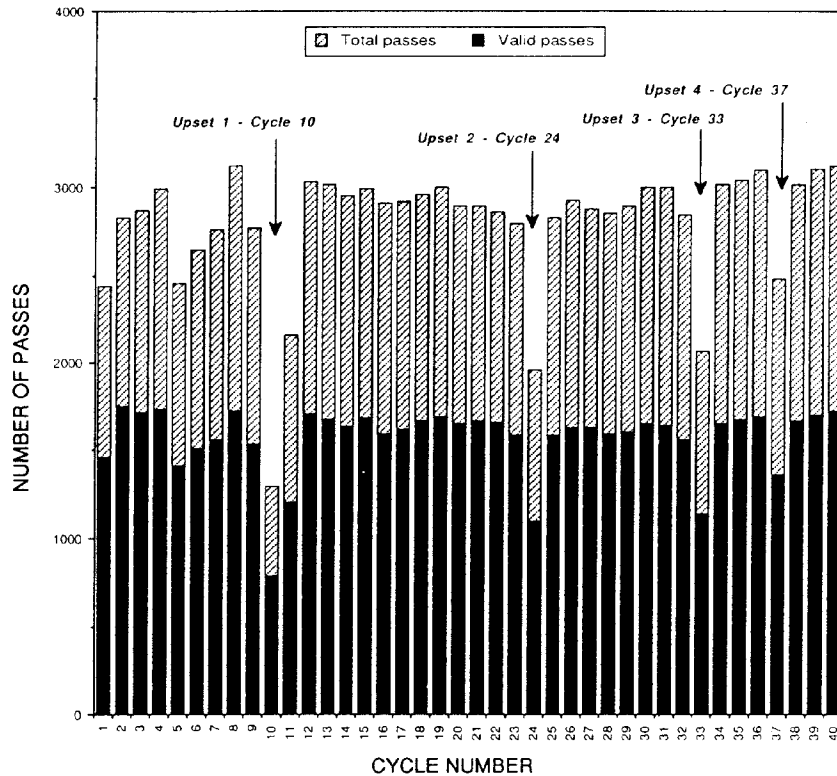


Figure 2. Number of observed passes per cycle during the first 40 cycles of T/P.

tional 1-day orbit at $D0 + 5$ (days are work days). CTDP is part of the CLS/Argos company which is running the DORIS system and the ZOOM software under CNES contract. This operational orbit has a 2-m RMS level quality on any component and for each of the current satellites. This operational setup was made available in January 1992 for SPOT 2 (more than fifty 10-day POEs delivered) and is currently utilized since cycle 1 of T/P.

3.3. The Orbit Determination Process

3.3.1. Frequency and time tag processing. One major problem with the one-way Doppler measurement is that there is no coherence between the received and reference frequencies (in contrast with a two-way link). To address the resulting frequency bias, ZOOM and other preprocessing programs such as the Guier algorithm [Guier, 1963] solve for one frequency offset per pass, which models the difference between the two USO frequencies. The master beacons are slaved to an atomic clock (a cesium in both Toulouse and Kourou). Therefore each adjusted frequency bias measured by Toulouse or Kourou can be considered as that attributable to the on-board USO frequency offset. The data time tagging is also performed through the two master beacons [Nouël et al., 1993].

3.3.2. Preprocessing. A two-step preprocessing is performed. First, passes with visibilities shorter than some criteria are eliminated and a low-elevation mask is applied to the measurements. The objective is to have reliable values for parameters estimated per pass. A few blunder points are also eliminated. Then, using the Guier formalism, ZOOM

solves for a frequency bias and two position offsets for each valid pass. By these steps, about 10% of the DORIS measurements have been eliminated.

3.3.3. Orbit processing. For each cycle of T/P, four POEs are computed. Two POEs are computed with only one type of measurement and two with both DORIS and satellite laser ranging (SLR) measurements: the very last one having the definitive Earth rotation parameters available from International Earth Rotation Service (IERS) rapid service. The complete dynamical and measurement configurations are given in Table 1. Between each orbit computation, various tests and editing processes are performed. They all are part of the orbit quality assessment.

3.3.4. Orbit quality assessment. Certain performance indices are displayed during each orbit solution to provide the operator with an initial check of the quality of the orbit: (1) an histogram of the residuals, (2) a time bias per pass converted into along-track offset, (3) the long-term fluctuation of these times biases obtained by subtracting a polynomial function of time, and (4) a spectral analysis of the resulting time series. In addition to these displays, internal and external consistencies of the POEs are evaluated. For T/P the internal consistency of the preliminary DORIS POE is evaluated using the following processes: a Guier algorithm using the preliminary DORIS POE and the corresponding Doppler residuals, including new data editing; an overlap with two 5-days arcs; an overlap with the previous cycle over 4 hours; a comparison with the ten 1-day operational CTDP orbits.

Table 1. Force Models and Parameters Used in POE Production

Orbit Determination Parameters	Values or Source of Data
Estimated parameters	Orbital state, solar radiation pressure coefficient (one per arc), drag coefficients (linear, two per day), three sets of Hill's coefficients (four per set), tropospheric biases (one per pass)
Integration type	Cowell order 10
Reference system	True of date
Integration step size	60 s
Satellite area model for drag/solar pressure	Box and wing model [Marshall <i>et al.</i> , 1992]
Satellite attitude	Computed from information on SAEI files
Geopotential model	JGM-2 (70 × 70) [Nerem <i>et al.</i> , this issue]
Solar and lunar attraction	Direct and indirect, BDL ephemerides
Solid Earth tides	$k_2 = 0.3 + \text{Wahr}$ [McCarthy, 1992]
Ocean tides	Schwiderski model [McCarthy, 1992]
Atmospheric density model	Drag temperature model [Barlier <i>et al.</i> , 1978]
Planetary attraction	Venus, Mars, and Jupiter, BDL ephemerides
Earth orientation parameters	IERS Bulletin D (see annual reports)
Station coordinates	JCOD4 (IGN) plus additions [Boucher <i>et al.</i> , 1993]

Abbreviations are SAEI, Satellite Attitude Event Information; JGM, Joint Gravity Model; BDL, Bureau des Longitudes; IERS, International Earth Rotation Service; IGN, Institut Géographique National.

Before processing a SLR-only POE, SLR residuals are computed using the preliminary DORIS orbit and editing is performed on the SLR measurements. After the processing of the SLR POE, the external consistencies of both are evaluated using the following processes: a computation of DORIS residuals using the SLR POE; a comparison between the SLR and DORIS POEs; a comparison between the SLR orbit from GSFC and our DORIS POEs; a comparison between the SLR orbits from both POD centers. The external consistency of our (DORIS + SLR) final POE is evaluated using the following processes: a comparison with the (DORIS + SLR)/GSFC final POE; a computation of altimeter crossover residuals.

3.3.5. Atmospheric refraction modeling. The dual frequencies of the DORIS system permit easily computable first-order ionospheric propagation corrections having good reliability. They are provided with the distributed DORIS data.

For the tropospheric propagation correction, the SOD uses a model specially developed for DORIS by the Centre National d'Etudes des Telecommunications which requires the knowledge of the meteorological parameters (temperature, pressure, and humidity). However, as a consequence of both model and meteorological data errors, and the existence of horizontal gradients in water vapor not sensed by local meteorological measurements, the tropospheric propagation correction is one of the dominant measurement error sources. This problem is mitigated through the solution

of a tropospheric bias per pass which scales the zenithal tropospheric delay.

3.3.6. Laser measurement modeling. The SOD had not processed laser data routinely before T/P launch. However, efforts were conducted during the SIP to verify SLR observation modeling. The SOD group is rapidly gaining insight into the global laser network including the station coordinates and the laser preprocessing characteristics. This problem was assisted through an agreement with the GSFC where laser data are provided for every T/P cycle which are preprocessed, including application of laser range array (LRA) corrections in the form of normal points. The availability of "clean" SLR measurements in this fashion helped the SOD to get good SLR performance: the laser RMS values have been plotted in Figure 3. However, more recently, SOD has developed improved laser preprocessing codes and introduced the LRA correction in the ZOOM software.

3.3.7. Reference systems and station coordinates. The subcommittee on standards of the T/P Science Working Team issued some recommendations about reference models or values which should be used for computing the satellite orbit. In general, one can say that all the T/P groups involved in precise orbit determination activity adopted these recommendations. Moreover, the software implementation of these models was cross-checked through the SIP.

Concerning the CNES orbit, the Internal Earth Rotation Service (IERS) reference system is adopted: International Astronomical Union (IAU) 1976 Precession and IAU 1980 Theory of Nutation. With respect to the terrestrial frame the DORIS station coordinates play an important role in the orbit accuracy, with 5-cm level positioning desired as identified in the error budget since the early days of the project. Before the T/P launch a fair amount of DORIS data on SPOT 2 satellite were provided to several groups who were going to be involved in the T/P precise orbit determination activity. Many investigations determined station coordinates for the DORIS network which were deployed at this time. These individual solutions were compiled by IGN and connected to the International Terrestrial Reference Frame (ITRF) [Boucher *et al.*, 1994]. Progressively, with the increasing number of DORIS beacons, new sets of coordinates were provided and we adopted solution JCOD4 for our POE. About 15 beacons are surveyed with respect to very long baseline interferometry or SLR sites, which enhances the connection to ITRF and allows the orbit to be computed uniformly with DORIS and/or laser mixed measurements.

The SOD has also computed several sets of DORIS station

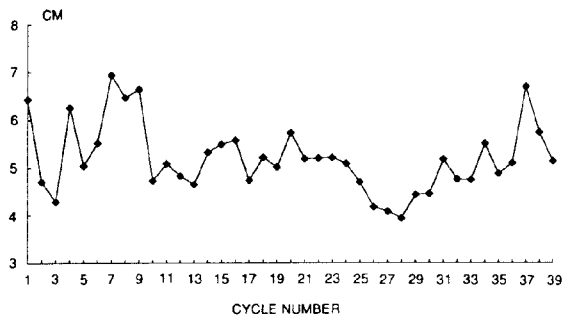
**Figure 3.** SLR residuals RMS with respect to CNES POE.

Table 2. DORIS Station Coordinates STP 93.0 Evaluated by SOD

Station	Coordinates			Internal Consistency, cm		
	X, m	Y, m	Z, m	North	East	Up
TLSA	4628047.611	119670.102	4372787.720	1.6	3.2	1.7
META	2890641.362	1310310.417	5513964.900	6.6	5.4	4.4
SAKA	-3465326.037	2638266.932	4644082.302	2.0	1.9	1.6
KITA	1945024.910	4556708.781	4004235.810	2.3	3.7	1.0
MANA	-3184357.580	5291042.190	1590419.393	2.8	5.9	4.2
HBKA	5084641.695	2670349.512	-2768497.095	2.4	5.1	3.1
MARA	3448405.861	2680356.249	-4632640.302	1.5	3.4	2.8
TRIA	4978463.193	-1086620.787	-3823205.524	1.7	2.3	1.7
HELA	6104828.380	-605837.594	-1740706.432	4.2	6.1	1.7
LIBA	6287388.618	1071573.969	39147.128	2.9	7.5	2.8
DJIA	4583119.629	4250951.957	1266247.716	2.3	4.8	3.1
YELA	-1224424.142	-2689227.492	5633645.207	5.0	3.5	2.2
GOLA	-2356504.009	-4646584.013	3668453.094	2.0	4.1	2.4
FAIA	-2282503.175	-1453416.978	5756694.479	3.2	3.3	1.4
KOKA	-5543974.762	-2054589.979	2387487.888	2.1	3.2	2.7
SODA	-2160725.256	-5643017.711	2034836.488	2.1	6.5	3.8
RIOA	1429849.894	-3495346.488	-5122723.065	2.3	2.3	2.3
EASA	-1884993.997	-5357604.965	-2892858.590	2.9	7.6	1.2
SANA	1776346.654	-5026544.303	-3491183.619	3.8	4.8	3.7
MORA	-5288462.754	3410034.692	-1038802.688	1.6	5.1	2.3
ROTA	909378.181	-2264934.606	-5872956.833	4.4	2.7	2.8
KERA	1405826.598	3918281.815	-4816203.946	3.3	2.0	3.1
AMSA	1086061.873	4927963.074	-3887828.077	2.2	4.3	2.7
ADEA	-1941059.582	1628659.521	-5833613.450	1.4	1.2	1.3
HUAA	-5345873.342	-2958239.081	-1824624.328	2.1	6.4	1.7
WALA	-6195393.699	-413727.903	-1454075.407	2.1	4.8	2.9
REUA	3364094.182	4907945.259	-2293482.257	3.6	5.6	2.0
SYOB	1766499.047	1460274.499	-5932211.610	2.1	1.1	1.4
RIDA	-960756.703	-5673685.205	2741529.464	1.6	4.5	2.0
YARA	-2389003.615	5043340.736	-3078513.173	3.1	4.1	2.3
ORRA	-4446470.430	2678102.128	-3696274.250	1.7	4.0	2.6
KRUB	3855261.113	-5049734.852	563057.803	6.4	7.8	4.7
REYA	2585528.319	-1044368.234	5717158.977	1.5	2.2	2.4
COLA	1113279.070	6233646.205	760276.632	2.1	3.7	1.9
DAKA	5886437.299	-1848461.672	1611441.723	3.1	4.7	2.5
FLOA	4221385.254	-2549305.908	4031509.201	2.7	5.0	1.7
BADA	-838277.474	3865777.112	4987626.631	2.2	2.3	2.3
GALA	42716.445	-6377216.438	-99590.648	1.6	3.5	0.6
Mean values				2.7	4.2	2.2

coordinates using the T/P orbit as a reference. A constraint was put on the orbit by holding fix the laser station coordinates, but let all the DORIS stations free, adjusting each station independently, that is to say simultaneously with no constraint on (or between) any of them. In this fashion a new set of coordinates is computed approximately every month (encompassing three successive cycles) during the first year of T/P lifetime. A set of 38 stations solution called STP 93.0 was produced. The internal consistency of STP 93.0 with respect to the monthly solutions is 2.7 cm for the north component, 4.2 cm for east, and 2.2 cm for height (Table 2).

This set has been evaluated with respect to JCOD5. The seven parameters transformation from JCOD5 to STP 93.0 solution are

- T1= 0.3 cm;
- T2= 1.3 cm;
- T3= -3.1 cm for translation;
- D= -0.22 × 10⁻⁸ for scale factor;
- R1= 0.06 milliseconds of arc (mas);
- R2= 0.37 mas;
- R3= -0.26 mas for rotation.

Although there is a noticeable offset on the Z component (T3 = -3.1 cm), the reference system is in good accordance with ITRF. However, if the north component difference is plotted versus the latitude of the station (Figure 4), there is an evident trend that likely corresponds to a bias on the inclination or equivalently to a systematic effect in the cross-track component of the T/P orbit. Assuming that JCOD5 is the standard with no such systematic error, this provides an external calibration of the cross-track component accuracy of the orbit, which is between 10 and 15 cm accuracy. Referring to the methodology proposed later on in section 6, the same order of comparison is obtained between the CNES orbit and that of the GPS-based orbit of the Jet Propulsion Laboratory (JPL). Slightly better comparisons ranging between 5 and 10 cm are seen with CNES and GSFC orbits for the cross-track component.

But what is the impact on the orbit of this new set of coordinates? In the orbit production scheme, one of the key tests of the expert system is to evaluate the amplitude of the twice per revolution spectrum line computed from the time bias values deduced from the DORIS measurement residu-

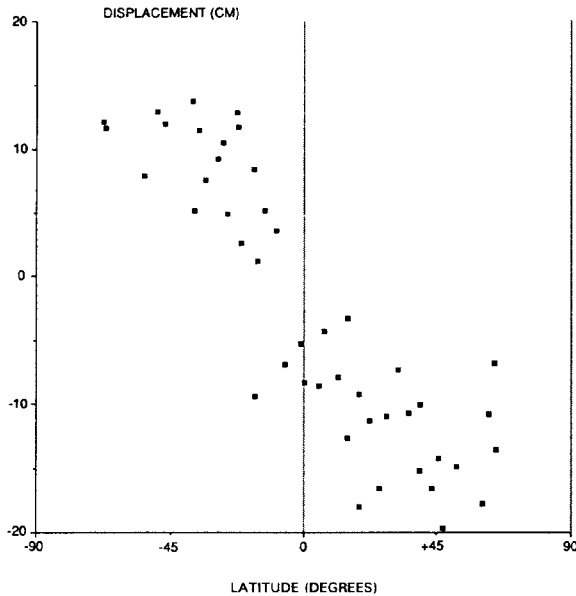


Figure 4. DORIS station displacements (north component) of STP 93.0 set with respect to JCOD5.

als. With STP 93.0, the amplitude at this line is considerably reduced.

4. Force Models

4.1. Gravity Field Selection

The fine tuning of the gravity field was one of the primary goals of the T/P validation period. Data from the first 15 cycles were processed by GSFC, CSR, and the GRGS to produce the Joint Gravity Model-2 (JGM-2) geopotential [Nerem *et al.*, this issue]. This field is used in all of the SOD T/P data processing.

Unfortunately, the ocean tide model associated with the JGM potentials are formulated in terms of sidebands based on solar and lunar osculating elements and cannot yet be modeled as such in our software. In place of the dedicated

tides we use the Schwiderski model [McCarthy, 1992]. Despite this limitation we have observed that each of the successive improvements of the gravity field lead to lower measurement residuals, better orbit overlaps, and lower altimeter crossover residuals. Also, the dominant effects of the tide model are long period and are thereby accommodated somewhat by empirical orbit parameters introduced in the solution. Tide model differences likely account for a significant portion of the cross-track difference seen between the GSFC and SOD orbits.

4.2. Nonconservative Force Modeling

Thanks to successive improvements in the gravity fields, geopotential errors have been significantly reduced. At the current level of accuracy, modeling of nonconservative forces has become the major concern for precise orbit determination, and extensive studies were conducted to improve the T/P model both before and after launch. Thermal and optical properties, as well as the exact size of the spacecraft, were carefully measured by Fairchild. These data were included in a detailed micromodel [Antreasian and Rosborough, 1992] to produce the exact reaction of over 300 components of the spacecraft to each of the radiative forces (solar radiation, Earth albedo, Earth infrared radiation, spacecraft infrared emission). Afterward, a simplified macromodel was developed [Marshall *et al.*, 1992], which retains most of the characteristics of the micromodel in the form of aggregate surface properties, consequently requiring a lower computation time.

The ZOOM software contains all of these sophisticated models. However, these models fail to accurately describe the actual nonconservative forces acting on the spacecraft beyond the 95% level, as can be seen from the unrealistic values of the estimated drag coefficients (C_D) (Figure 5). The unexplained force acting on T/P, commonly called the "anomalous" force, represents about 5% of the predicted nonconservative force. It was shown soon after launch that this force was unexpected and is body fixed. However, its origin has not been clearly established as of this date. Fortunately, a detailed understanding of this force is not required for precise orbit determination, for its clear manifestations can be accommodated through empirical modeling.

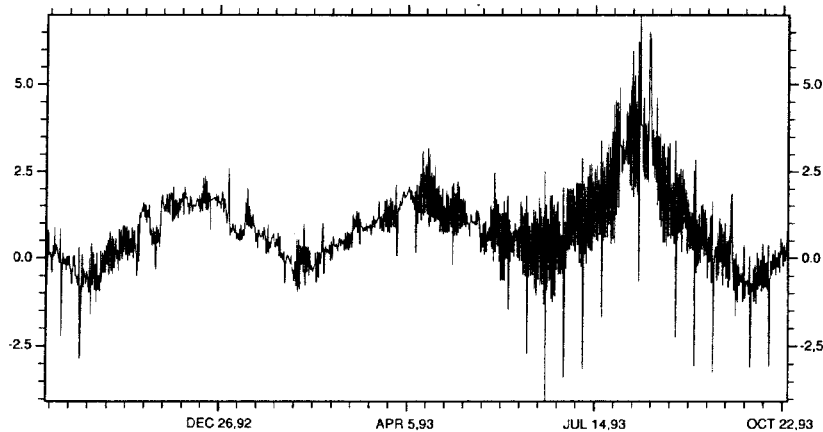


Figure 5. Empirical drag factors estimated every 12 hours.

4.3. Empirical Force Modeling

Once it was established that empirical parameters had to be solved for, the decision was taken to limit the surface force model to direct solar radiation and drag. These forces present the advantage of being relatively well known, and they account for about 85% of the predicted nonconservative force. The remaining unmodeled forces are absorbed by the empirical coefficients along with the anomalous force. This strategy was adopted for it saves a significant amount of computer time with no resulting orbit degradation.

The actual goals in our efforts do not require explicit modeling of all forces, but rather, to model their impact on the orbit. During the first few months of operation, studies were conducted by the SOD to find a strategy to remove the effect of any unmodeled force on the orbit. This effort is greatly enhanced by the dense temporal coverage provided by the DORIS network. In order to properly evaluate the effect of various techniques, DORIS and SLR residuals were converted into time biases (which are used to assess along-track orbit error). Amplitude periodograms of the resulting time series were compared. Because of the small number of data points, periodograms of SLR data do not cover a large enough frequency range to be meaningful. However, the frequency analysis of DORIS residuals is very instructive. Periods from a few days to about 4 cycles per revolution (cpr) can be observed with excellent signal to noise ratio. And thanks to the repeatability of the time distribution of DORIS measurements from cycle to cycle, periodograms can easily be compared over long periods of time.

Empirical drag factors (C_D) are almost always solved for during orbit restitution in order to mitigate the deficiencies of the atmospheric density models. It is also well known that these factors absorb other unmodeled forces acting on the spacecraft in the along-track direction. It is then only a matter of observability to determine how many such coefficients can be solved for in a given arc. In the case of T/P, the atmospheric drag is very small due to the high altitude of the spacecraft and the current low level of solar activity. As the observability of the empirical coefficients diminishes with the intensity of the force decreasing, "DORIS only" orbits produced by the SOD include only one C_D per day. However, this induces a strong one per day signal in the time-bias residuals. When SLR data are added in the computation of the POE, there is enough data to be able to solve for two C_D parameters per day. With this configuration, the one per day line disappears from the periodograms, while introducing a much smaller signal at the twice per day period. However, these coefficients are obviously not physically tied to atmospheric density errors (Figure 5).

Hill's equations theory [Colombo, 1989] describes the dynamical motion of a spacecraft in terms of a filter. Whatever the frequency spectrum of the perturbation forces, the only frequencies which appear in the orbit are either very low or close to once per revolution [Cretaux et al., 1994]. Hence in terms of its action on the orbit, any perturbation can be approximately replaced by an acceleration whose period is equal to the orbital period. In practice, empirical forces at the osculating period of the spacecraft are added in the along-track and cross-track directions. These forces are applied as constants in amplitude and phase over some specified orbit interval and are solved for during the orbit determination process. The cross-track term is utilized to

accommodate any normal error, while the along-track term absorbs any transversal or radial error.

This process is successful as seen in the removal of the bulk of the signature at once per revolution in the time bias residuals. However, the force modeled by these Hill's accelerations is a surface force which is spacecraft body fixed and consequently is directed in a different direction on orbit depending on the attitude of T/P, and whose signature is therefore a function of the attitude law of T/P. When the attitude law changes the character of the 1-cpr error also changes. It was quickly noticed that when the Hill's parameters were not covering periods of time which did not coincide with the actual attitude law, the once per revolution peak in the time residuals not only did not disappear but it also splits into two very close peaks. This reflects the dependency of the anomalous force on the attitude law [Frauenholz et al., 1993]. To account for changes in the attitude law, a new set of empirical Hill's coefficient is solved for each period. The middle of the ramp up, ramp down, or flip periods is used to delimit the intervals over which the coefficients are constant. Thus there are as many sets of Hill's factors as there are attitude law changes during each cycle. Up to now, no more than three different attitude regimes were observed during one T/P cycle.

The increase in the employment of empirical parameters naturally decreases the RMS of the residual fit to the tracking data. But if properly applied, they also improve the quality of the orbit by several centimeters on the along- and across-track RMS values as can be judged by the various internal validation tests. Thus in order to maintain a good observability of the coefficients while improving the orbit, we have found that three sets of Hill's factors are needed to be solved for over any arc, even when there are no changes in the attitude law.

5. Orbit Accuracy Validation

One of the main tasks of the orbit production system at CNES is to validate its products. To do this, various techniques have been developed. First, the CNES POE quality is evaluated internally, by evaluating the tracking data residuals and comparing the DORIS and SLR orbits. Then it is evaluated externally, by computing altimeter cross-over residuals and through comparisons with the GSFC POE.

5.1. Internal Validation

Figure 6 displays the total RMS of the DORIS residuals per arc along with the postfit Guier detrended residuals.

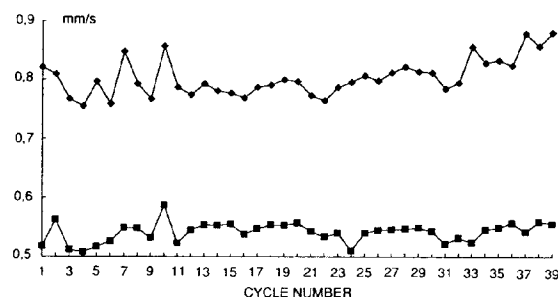


Figure 6. DORIS residuals RMS: Guier formalism (squares) and with respect to CNES POE (diamonds).

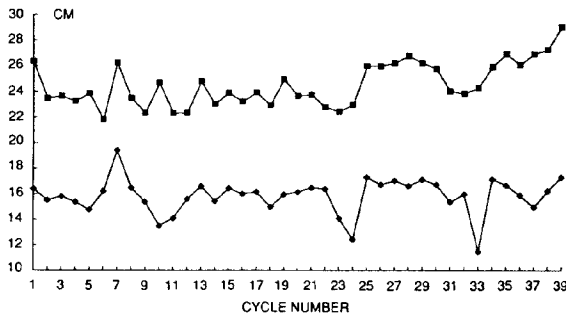


Figure 7. Along-track (squares) and slant range (diamonds) RMS computed from DORIS residuals with respect to CNES POE.

Guier residuals are typically around 0.5 mm/s, close to the actual instrument noise, while DORIS residuals are of the order of 0.8 mm/s. The difference reflects the fact that frequency biases are estimated during Guier processing, while they are kept fixed during the orbit determination. This difference also reflects other actual orbit errors due to multiple sources of lower amplitude. Thus the DORIS residual cannot be directly mapped into orbit accuracy. Corresponding RMS of fits to the SLR data are shown on Figure 5. Laser residuals represent an absolute range standard, so their level of about 5 cm is an upper bound for the actual radial orbit error.

Figure 7 displays the RMS of the Guier offsets in the slant and along-track directions. Here again the offsets in the slant direction incorporate station location and tropospheric delay errors along with actual orbit errors. Thus these results offer a good estimate of the total measurement modeling but they only provide a rough estimate of the orbit quality.

It should be noted that the fine structure of the variation of the RMS of the Guier residual from arc to arc (Figure 6) is not completely random. The signature for cycles 9 through 13 repeats itself for cycles 22 through 26. Not surprisingly, the changes in the attitude law are similar for both periods. Moreover, the two cycles 11 and 24, which correspond to the lowest residual, are the only cycles with fixed yaw over the whole cycle. This shows that during fixed yaw periods, when the effect of the anomalous force on the orbit is maximum [Frauenholz *et al.*, 1993], the empirical model is the most effective. In turn this demonstrates that if a good model of the anomalous force over all attitude laws was available, the residual level could be reduced significantly to that observed during cycles 11 and 24.

A second important tool for internal orbit validation is the direct comparison of various orbit solutions obtained from different data sets covering the same time period. In each case the variable of interest is the RMS of the orbit difference in the radial direction. Figure 8 shows the results of four such tests. Triangles represent the RMS difference between the POE and the "DORIS only" orbit. This difference fluctuates depending on the availability of DORIS data. At times of DORIS data outages, the "DORIS only" orbit diverges with respect to the POE (when the triangles are higher than all the other symbols). Open circles represent the RMS difference between the POE, and the "SLR only"

orbit. These two tests provide an estimate of the bias in the POE induced by either data set. The results are very similar and consistently at the 2-cm level.

Diamonds in Figure 8 represent the RMS differences between the POE for cycle $n - 1$ and for cycle n in the 4 hours period where they overlap. Their level is also at the 2- to 3-cm level, showing that the traditional deterioration of the orbit at each end (bow tie effect) has been contained. Squares display the RMS difference between the POE and ten 1-day orbits computed using the same data set. This difference enhances the contribution of long-term model errors, which are absorbed in the frequent adjustment of orbit state variables and therefore should not show up in the single-day arc solutions. Here again, differences are at the 2- to 3-cm level. The whole set of internal validation tests shows that the consistency is at the 2- to 3-cm RMS level indicating that the orbit noise in the radial direction is below 5-cm RMS.

5.2. External Orbit Validation

5.2.1. Crossover residuals.

Altimeter crossover residuals provide an interesting estimate of the orbit quality for many reasons. First, it is a truly independent assessment since the altimeter data are not used to produce the orbits. Second, these data evaluate the orbit quality in the radial component directly.

The comparison of the RMS altimeter crossover residuals obtained from various orbits offers an insightful way to compare the accuracy of the different solutions for a given data arc. Figure 9 compares the altimeter crossover residuals computed with the CNES POE and the GSFC POE. It clearly shows that the quality of both of the orbits is nearly identical for practical purposes. It should be stressed that crossover residuals from arc to arc do not directly reflect orbit quality alone, but rather contain strong signals like mismodeled ocean tides and nontidal. Therefore altimeter crossover tests on T/P are more suitable for blunder detection, taking into account the fact that the actual orbit accuracy is well below the RMS of crossover residuals. Crossover residuals with JPL orbits are not included here, for they were not produced within the time frame of our validation procedure.

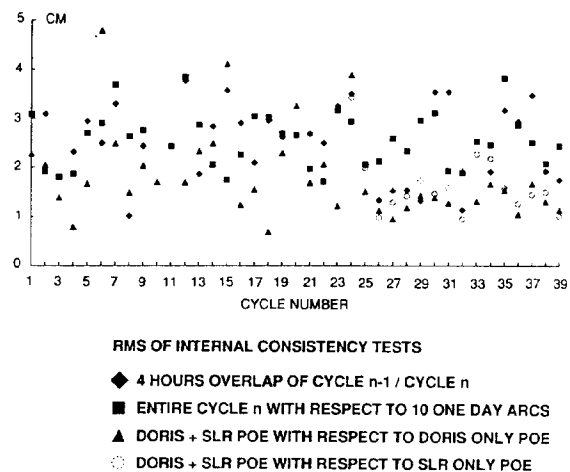


Figure 8. RMS of internal consistency tests.

5.2.2. Ephemeris comparisons with GSFC. The CNES POE and NASA POE are continuously exchanged. The two orbits are systematically compared by the SOD expert system before any final orbit delivery. The RMS orbit differences in three components over each cycle represents a key test at the present time (Figure 10).

For the radial component, the mean RMS difference value over the T/P lifetime is 2.5 cm. It is around 6 cm for the cross-track component and around 10 cm for the along-track component. These comparisons do not reflect the tracking data measurements (DORIS and/or laser) for they are used in common. Sometimes there are jumps in the comparisons which correspond to the fact that with the same data the orbits are computed with different strategies and software. However, accompanied by excellent fits to the data, these results reveal a high level of orbit performance.

Tests have been conducted on cycle 14 where only DORIS tracking data fits were performed with CNES, GSFC, and JPL orbits: they all agree within 0.04 mm/s, which is not significant compared to an instrumental DORIS noise of 0.3 mm/s. Concerning the radial component, there seems to be long-term period in the RMS resembling “arches,” but no further investigation has explained their appearance.

6. Fundamental Concepts When Comparing Orbits

In practice, an orbit is given to the users as sampled time series of the six components of the position/velocity vector. Moreover, given two such orbits, their difference can be mapped into the classical along-track, across-track, and radial components. In the case of TOPEX/POSEIDON, as the radial component is the major concern of the mission, it is of common practice to report the RMS value of these differences over the 10-days cycle in order to compare orbits. However, there is an evident coupling between the along-track component and the radial one coming from the third Kepler law. Also, orbits are commonly computed through a filtering process which adjusts all six components of the initial state vector. This is the reason why this section is not limited to the radial component although it is the focus of the discussion herein.

Another important issue comes from interpreting these differences as an estimate of the actual accuracy of the orbit. There are some common errors to the two orbits that will cancel when computing the difference, but this fact is mitigated because the strategies, tracking measurements, or

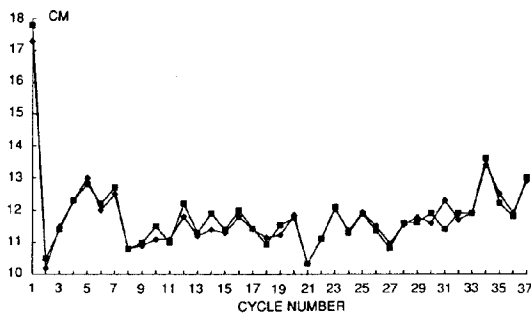


Figure 9. Crossovers residuals computed from CNES POE (diamonds) and NASA POE (squares).

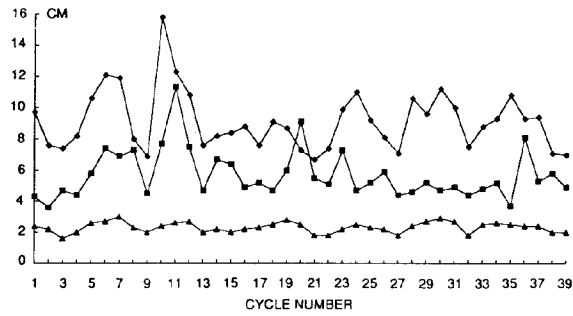


Figure 10. CNES and GSFC comparisons RMS in along-track (diamonds), cross-track (squares), and radial (triangles) components.

software for evaluating the orbit vary from one group to another. So, to the level of a few centimeters accuracy, it becomes increasingly more important to develop a more rigorous method of comparison and not to characterize it by only one number, that is to say, the RMS over 10 days.

6.1. Statistical Hypothesis

When the difference of two orbits $\rho_1(t)$ and $\rho_2(t)$ on one of the components is plotted with respect to time, one can consider that it is a realization $\delta\rho(t)$ of the error on that component and it can be represented as a random process. Such a realization almost always exhibits a strong periodic component at once per revolution. Several studies [Colombo, 1989; Engelis, 1987] have shown this once per revolution period, which is a natural phenomenon if the satellite motion is looked at as an oscillator with a proper frequency equal to the orbital frequency. In addition, there are several other frequencies which can be seen in the low-frequency spectrum; the corresponding periods of the order of several hours or more are visible mainly on the along-track component, but a Fourier analysis confirms that they are also present in the other components.

The stationary hypothesis has to be considered when analyzing the time series. The motion of the satellite is subject to a large spectrum of perturbations. For a circular orbit, it has been shown that the gravity field produces effects which are geographically invariant on the three components [Rosborough, 1986; Melvin, 1988], that is to say, independent of time and close to stationary [Kaula, 1966]. So, as seen from a time series point of view, the statistical means, or expected values, and the time average means are only equivalent if the ergodicity principle is verified, which implies a stationary process. Consequently, the approach will be to achieve as closely as possible this necessary condition, before any RMS estimate. The other error sources, coming from nonconservative forces, for example, will refute the stationary hypothesis and will produce long-term trend as well as a modulation at the once per revolution frequency. In order to overcome these interactions, we will try to separate the long term (shift) from the short term (distortion).

6.2. Shift and Distortion

Borrowing from some ideas coming from the pointing stability problems [Lucke et al., 1992], the total error $\delta\rho(t)$ is decomposed into two components: a shift $s(t)$ (sometimes called drift, but very often this term represents a polynomial

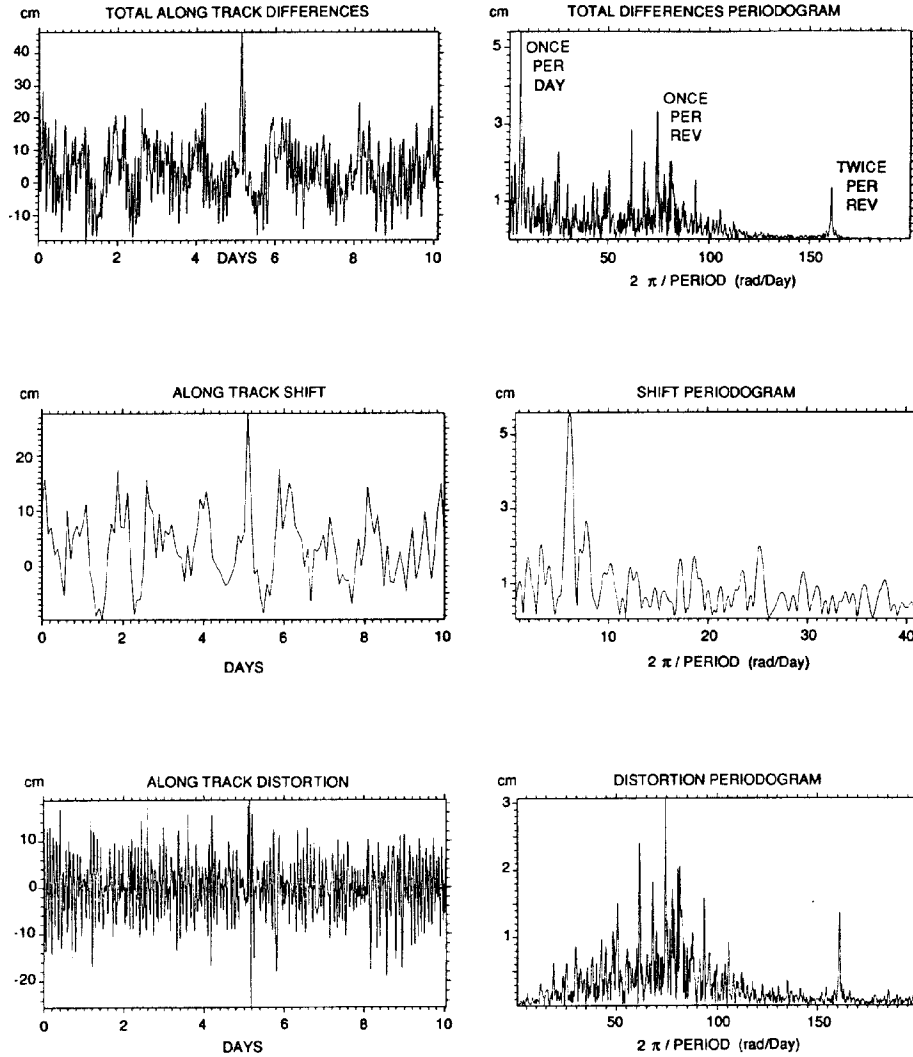


Figure 11. Example of separation between the long-term component (shift) and the orbital period component (distortion) for CNES POE-JPL orbit (cycle 25).

trend) and a distortion $d(t)$ (also called jitter). The difference $\delta\rho(t)$ seen as a potential realization of the error, is supposed to have zero mean over the entire 10 days cycle for further analysis. If not, this bias is easy to evaluate and to subtract it from the signal. Biases should be controlled from one cycle to the other, and it is done by the current exchange of orbits between GSFC and CNES (for example, we have an 0.8-cm bias on the radial component between the CNES POE and the NASA POE which is stable from cycle to cycle since cycle 1). Let T be the orbital period, or close to it (eventually it could be the time separating two successive ascending crossings of the equator).

The shift over T is defined as

$$S(t_i, T) = \frac{1}{T} \int_{t_i}^{t_i+T} \delta\rho(t) dt$$

where $t_i = t_0, t_0 + T, t_0 + 2T, \dots$ in the case presented here, in order to limit the computations. It can be extended as a running average to get a continuous function $s(t)$.

The instantaneous distortion $d(t, t_i, T)$ is defined by

$$d(t, T) = \delta\rho(t) - S(t_i, T) \quad t_i < t < t_i + T$$

Obviously, the mean value of d over every $[t_i, t_i + T]$ intervals is zero. It is this definition of the distortion that will be analyzed later on, even if it is a noncontinuous function of time due to the chosen value of the shift.

We note one important fact: if the mean square value of the distortion is taken over T , that is to say,

$$D^2(t_i, T) = \frac{1}{T} \int_{t_i}^{t_i+T} [\delta\rho(t) - S(t_i, T)]^2 dt$$

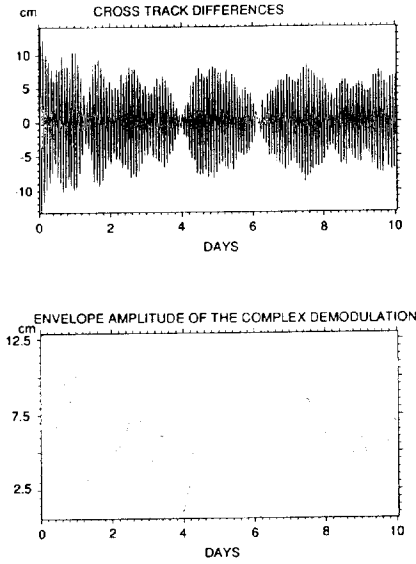


Figure 12. Example of the use of complex demodulation to extract the once per revolution modulation for CNES POE-GSFC POE (cycle 18).

$$D^2(t_i, T) = \frac{1}{T} \int_{t_i}^{t_i+T} \delta\rho^2(t) dt - S^2(t_i, T)$$

$$D^2(t_i, T) = E^2(t_i, T) - S^2(t_i, T)$$

the total mean square error $E^2(t_i, T)$ is decomposed into a couple of almost orthogonal (on a quadrature basis) errors such that

$$E^2(t_i, T) = S^2(t_i, T) + D^2(t_i, T)$$

The low frequencies have little influence on the distortion which is itself sensitive to the high part of the spectrum (the inverse being true for the shift). When an orbit is estimated with dense tracking coverage, several parameters are adjusted to take care of surface forces, causing a reduced shift (diminishing the classical “bow tie” shape). Parts of some long-term gravity perturbations are probably absorbed in these parameters, but it is fundamentally the precise orbit which interests oceanographers as long as they are also given the corresponding spectrum irrespective of how the orbit has been obtained. Both types of errors need to be understood: the long term or shift for topography and the short term or distortion when using several orbit arcs over an ocean.

In order to illustrate the application on an actual case, the differences on the T/P along-track component have been plotted versus time (Figure 11). The orbits compared are the JPL orbit (with GPS and the “reduced dynamic” technique) and the CNES orbit (with laser and DORIS) over the entire interval of cycle 25. As it is defined above, the corresponding shift and distortion are also plotted, with the associated periodograms. One can see that the shift has a clear once per day spike; the distortion contains several spikes around the once per revolution plus a sharp twice per revolution line. Concerning the twice per revolution effect, one should

remember that JPL solves for several twice per revolution coefficients in their “reduced dynamics” approach, whereas CNES does not. Both orbit estimation schemes are adjusting coefficients for the once per revolution term.

More than 15 cycles have been treated in this way and have been evaluated in each orbit component. Most of the time, the initial periodogram exhibits a shape similar to the given example with shift and distortion revealing separate long-period (several days to several hours) from short-period effects (a few revolutions to parts of revolution).

6.3. A Proposed Model for Distortion

The distortion is a zero centered process and at a first glance, it looks like harmonic oscillations close to the orbital frequency, with random amplitudes. The corresponding periodogram shows several harmonics around the once per revolution term and can be ascribed as a narrowband spectrum around it. That kind of random process can be modeled by an expression such as [Levine, 1973]

$$d(t) = a(t) \cos \omega_0 t + b(t) \sin \omega_0 t$$

where $a(t)$ and $b(t)$ are normal stationary random processes with variance σ^2 , and $\omega_0 = 2\pi f_0$ where f_0 is any frequency value close to the orbital frequency (which should have a constant value only in the ideal Kepler case).

The distortion can be written

$$d(t) = \alpha(t) \cos [\omega_0 t + \phi(t)]$$

with an envelope

$$\alpha(t) = [a^2(t) + b^2(t)]^{1/2} \quad \alpha \geq 0$$

and a phase

$$\phi(t) = \arctan [b(t)/a(t)]$$

So, this process is interpreted as a carrier frequency (f_0) with amplitude and phase modulations varying slowly with time compared to $\cos \omega_0 t$, so that their spectra would be in the low-frequency domain.

The density function of the envelope is given by the generalized Rayleigh distribution [Levine, 1973]

$$w(r, t) = \frac{r}{\sigma^2} e^{-(r^2 + \alpha^2(t))/2\sigma^2} I_0\left(\frac{r\alpha(t)}{\sigma^2}\right)$$

with I_0 being the zero-order Bessel function with imaginary argument. This distribution depends upon two parameters $\alpha(t)$ and σ and the shape of the curve upon the ratio $\alpha(t)/\sigma$ (σ is independent of time).

When there is no modulation ($\alpha(t) = 0$), it means that a noise level has been reached below which no further information can be detected. In other words, no refinement is possible in terms of deterministic model for the two orbits which are compared. In the case of the 2-cm challenge, this σ would be 2 cm.

When $\alpha(t) \neq 0$ and $\alpha(t)/\sigma \geq 4$, the Rayleigh distribution is approaching a normal distribution with mean value $\alpha(t)$; in other words, for the two orbits which are differenced, we have a systematic difference in one of them. This information could be further analyzed and mapped to be geographically correlated, for example.

The envelope $\alpha(t)$ is computed using the complex demodulation technique which gives access to $a(t)$ and $b(t)$ [Fran-

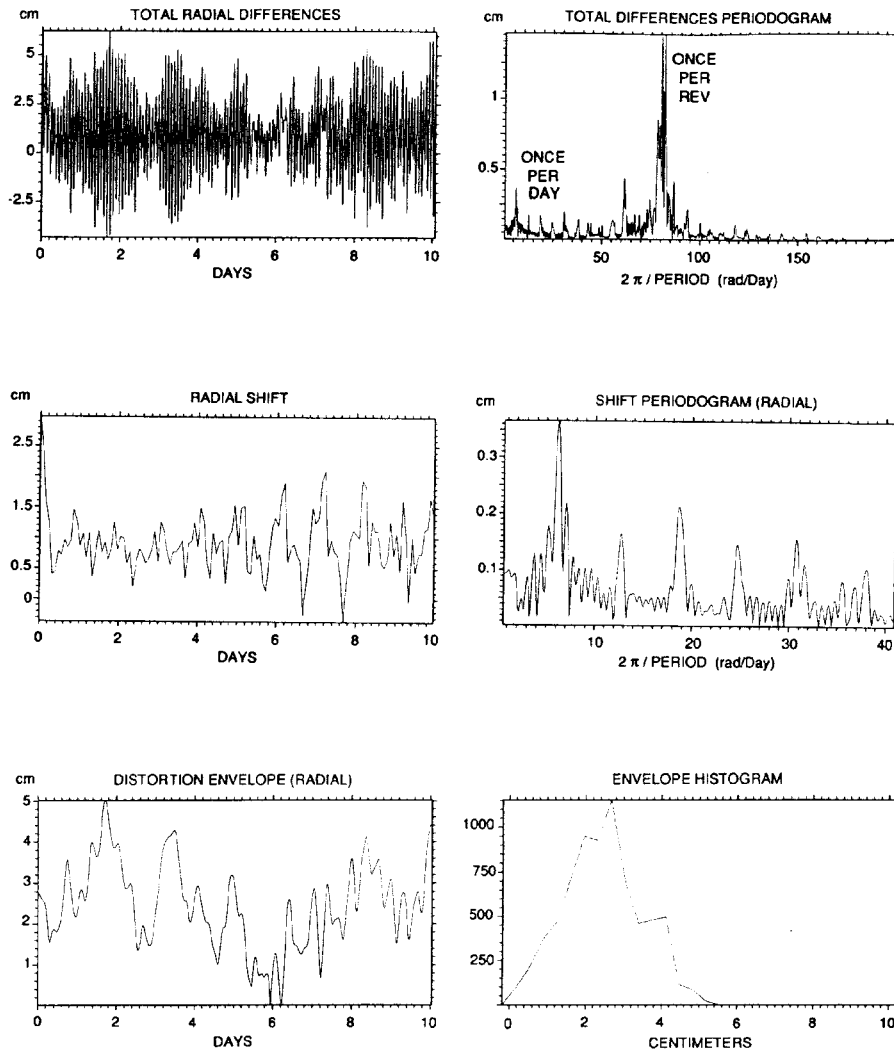


Figure 13. Cycle 14 (CNES POE-GSFC POE) radial differences. Analysis of the shift and the distortion.

cis and Bergé, 1993]. The phase $\phi(t)$ is sometimes difficult to compute when the original signal is close to zero. Part of this problem is solved by comparing two successive values [Wan *et al.*, 1990].

As an example, the cross-track difference between the GSFC and the CNES orbit for cycle 18 is presented in Figure 12. The envelope $\alpha(t)$ slowly varies with time. Its histogram is approaching a Gaussian distribution with a mean of 6.1 cm and a standard deviation of 2.1 cm. In other words, the error can be described by a vector, with a length of 6 ± 2 cm which rotates at the orbital frequency, irrespective of the phase of this vector. If we had taken the time average over the entire cycle of the original signal, it would have been close to zero.

6.4. Application to the Radial Component

Up to this point, only a few examples have been given to support this comparison method. A thorough analysis has been performed over 16 cycles between the GSFC and the CNES orbits which are provided with the GDR. These orbits

encompass the entire 10 days duration, but the cycles were selected on the availability of the JPL-provided ephemeris files computed using GPS data at the time when the comparison was initiated. At this time cycles 22, 23, 26, and 27 were limited in duration from 3 days to 8 days in these JPL-derived files. A bias of about 1.5 m in the along-track component shows up for cycle 26, 27, 28, and part of 29 when compared to the CNES orbit and has been explained by the adoption of a poor clock standard in the GPS orbits; there is no such bias with the GSFC orbit. However, in these cases the JPL orbits seem to be reported simply in an offset time system which might alter the random variations seen about this offset, at least along track. It is difficult to ascertain the consequences on the corresponding radial component.

All the procedures presented above have been applied to $\delta\rho_1(t) = \rho_{\text{CNES}}(t) - \rho_{\text{GSFC}}(t)$ and $\delta\rho_2(t) = \rho_{\text{CNES}}(t) - \rho_{\text{JPL}}(t)$ which are tabulated every 60 s and can be considered as representing two realizations of the error on the radial

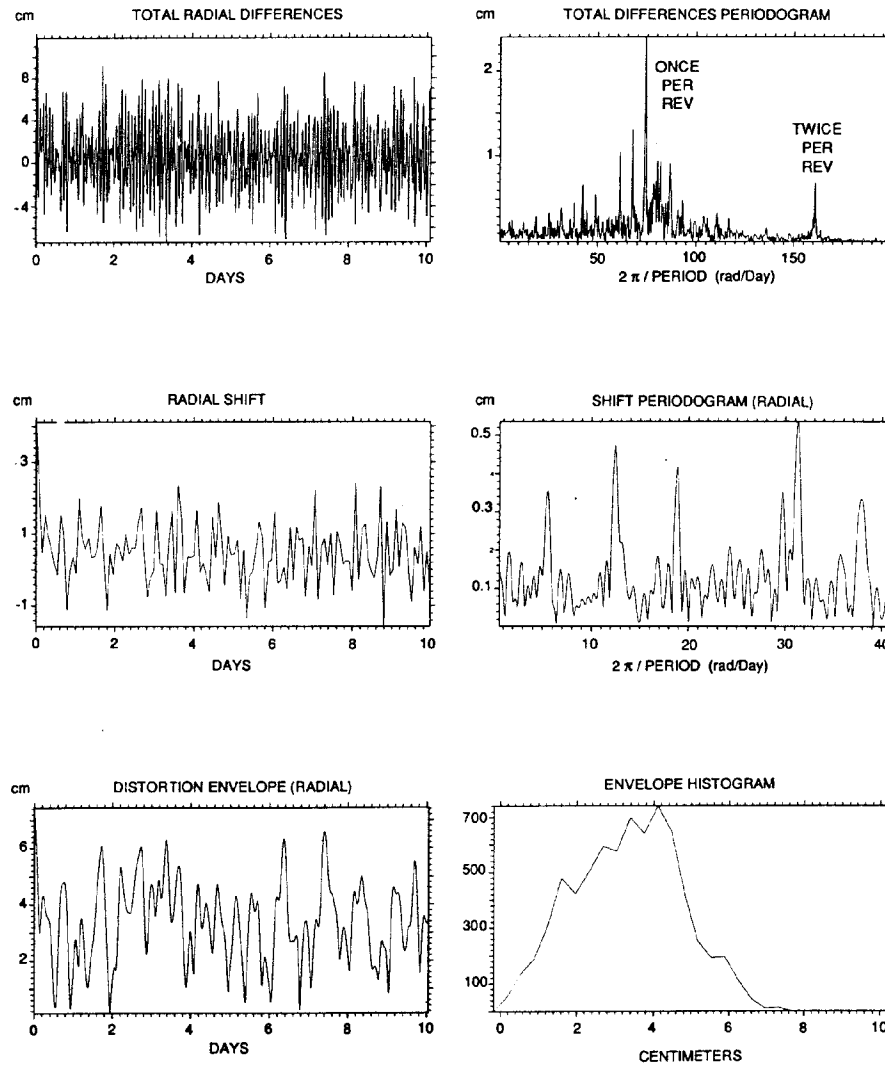


Figure 14. Cycle 14 (CNES POE-JPL POE) radial differences, Analysis of the shift and the distortion.

component. Only a synthesis of the results will be given, and features which are present in all the cycles will be mentioned and illustrated with cycle 14.

Concerning the periodograms of $\delta\rho_1$ and $\delta\rho_2$, the values of the highest spike varies within a 5-min band around the 112-min orbit period for $\delta\rho_1$ (GSFC) and surprisingly within a 10-min band around 122 min for $\delta\rho_2$ (JPL) (Figures 13 and 14). This suggests that it is insufficient to consider a single fixed period (e.g., the orbit period) and to consider the problem as a narrowband random process. Evaluation techniques which assume an a priori constant value for the period should likewise be avoided. Concerning the average over all the cycles of the main spectral line amplitude, it is 1.7 ± 0.5 cm for CNES-GSFC and 2.2 ± 0.3 cm for CNES-JPL. It should be noted as expected that only with the JPL orbit we do see a significant twice per revolution line.

Concerning the shift, for the CNES-GSFC comparison, the main line is around once per day with an average

amplitude of 0.3 cm. Several other lines are seen at 4, 5, 6, 8, and 12 hours, the amplitudes of which are below 0.2 cm, but vary from one cycle to the other (Figure 13). When studying the shift for the CNES-JPL comparison (Figure 14), the main spectrum line is precisely one of these 4, 6, or 8 hours line with an average amplitude of 0.5 cm. There is no evident explanation for the absence of the once per day signal given it is an important natural spectrum line associated with the daily terms of the gravity field perturbation. A possible explanation, although not obvious, may be found in the fact that the CNES and GSFC orbits are estimated over the entire 10-day cycle, whereas JPL orbits are fitted over arc lengths of only 30 hours. In both cases, the histograms corresponding to the shift are normally distributed with a mean of 0.8 cm and a standard deviation of 0.4 cm for CNES-GSFC (respectively 0.5 cm and 0.8 cm for CNES-JPL).

The comparisons concerning the distortion were also thoroughly evaluated and statistics about the envelope are

Table 3. Distortion Envelope on the Radial Component

Cycle Number	CNES-GSFC		CNES-JPL		Satellite Attitude*
	Mean	σ	Mean	σ	
10	2.8	1.3	3.6	2.0	S/F
14	2.4	1.0	3.3	1.4	S
15	2.2	0.9	3.5	1.5	S
17	2.7	1.0	3.6	1.6	S/F
18	3.0	1.3	3.6	1.9	F/F/S
19	3.5	1.3	2.8	1.4	S
20	2.7	1.5	3.9	2.1	S
21	1.9	0.7	3.3	1.6	S
22	1.8	0.9	3.8	1.5	S
23	2.3	1.1	4.0	1.5	S/F
24	2.8	1.5	3.5	1.7	F/F
25	2.5	1.4	2.9	1.4	F/S
26	2.4	1.2	3.2	1.3	S
27	2.0	0.9	3.3	1.4	S
28	2.7	1.5	3.1	1.3	S
29	3.2	1.4	3.4	1.8	S/F/F
Mean	2.6	1.2	3.4	1.6	

Units in centimeters.

*Yaw angle motion law: S, sinusoidal; F, fixed.

displayed in Table 3. The shapes of the envelope and the corresponding histograms are plotted in Figures 13 and 14. One can notice that the CNES-JPL values are higher than those of CNES-GSFC, except in the unique case of cycle 19. If one supposes that the error can be represented by a vector rotating at the orbital frequency, the length of that vector is 2.6 ± 1.2 cm (1σ) in the case CNES-GSFC and is 3.4 ± 1.6 cm (1σ) in the case of CNES-JPL.

After removing the shift and the distortion from the original time series, it is interesting to see what is left. In the case of CNES-GSFC the remainder is Gaussian white noise (i.e., no deterministic signal at any frequency with an amplitude higher than 0.1 cm). The mean value is zero and the standard deviation is 0.3 cm. The same evaluation of the CNES-JPL residual signal finds Gaussian noise with a mean value of zero and a standard deviation of 1 cm. Moreover, as expected, it is not a white noise: the twice per revolution spectrum line shows up with an amplitude of 0.7 cm. The analysis might have been carried on for that typical frequency, but it is not clear if it represents an actual orbit error. These remaining errors have been geographically mapped. There is no evident geographic correlation with CNES-GSFC; on the contrary, a region of residuals lower than -4 cm is located in a part of the South Pacific Ocean for the CNES-JPL comparison; this seems to correlate with the expected errors from JGM-2 [Christensen *et al.*, this issue]. A vague band around the equator has residuals between 0 and 2 cm and between 0 and -2 cm with increasing latitudes (which probably is attributable to the twice per revolution effect).

6.5. How to Compare Orbits to Centimeter Level

In summary, the RMS statistic of the difference of two orbits over the entire cycle is not enough to represent the error at the 2-cm level. We suggest, since the orbital frequency is a fundamental one, one should separate the error into two orthogonal components over the orbital period, namely the shift and the distortion, such that their root-sum-square gives the total error at this frequency. The shift is characterized as containing only terms with periods lower

than 2 or 3 orbital periods. The distortion, having several spectrum lines around the orbital frequency, is modeled as a rotating vector. The amplitude of this vector can be estimated and its mean value and standard deviation statistically computed irrespective of its phase; the radial error can then be reported as having a mean error of $x \pm y$ cm (1σ). These procedures are coherent with the way orbits are computed. Although these thoughts are preliminary and require further analysis, it seems that they provide a good starting point for providing a standard way of comparing orbits to the level of a few centimeters accuracy.

7. Conclusion and Future Works

It has been shown, with a tremendous prelaunch and postlaunch modeling effort, that the 10-cm level on the radial component can be achieved as part of a production process. The current tests prove that an even better accuracy is reached, around 3 to 4 cm for T/P [Tapley *et al.*, this issue]. To deal with such small error estimates, it becomes apparent that new statistical methods devoted to orbit accuracy assessment are needed. An attempt to define such approach along with its statistical metrics has been proposed, but it requires further investigations.

The French DORIS system has been shown as a very valuable contribution to the altimetric mission. The same expert system is used by the Service d'Orbitographie DORIS to produce and evaluate orbits. Coupled with the 2 to 3 cm given by our expert system and obtained at the TOPEX/POSEIDON altitude (to be compared to 4 cm predicted with JGM-2), a 5-cm value is reached with the DORIS measurements tracking on SPOT 2 and SPOT 3 at an altitude 832 km (to be compared to 8 cm predicted with JGM-2 [Nerem *et al.*, this issue]). Future applications of DORIS are planned for SPOT 4 [Berthias *et al.*, 1993], ENVISAT (European polar platform), and TOPEX/POSEIDON Follow On.

The highly accurate TOPEX/POSEIDON results would never have been obtained without the improvements of the JGM gravity models. These developments were extensively used by the scientific community, whatever tracking data they process. For future missions, tuning of new models will probably be necessary, according to the corresponding orbit. However, the almost continuous coverage of the orbit by the DORIS network allows such an effort to be efficiently accomplished, bringing new contribution to this field. Moreover, as was proven with the "anomalous" force acting on the TOPEX/POSEIDON spacecraft, the dense coverage of DORIS allows artful filtering techniques to be applied in order to monitor and recover nongravitational perturbations.

Acknowledgments. The work described here was performed by the Service d'Orbitographie DORIS. Besides the U.S.-French TOPEX/POSEIDON project and the CNES DORIS project, whom we thank for providing us with this accurate and exciting material, we are grateful to the CNES Division Mathématiques Spatiales and directorate Traitement de l'Information for their continuous support, in particular for providing us with large-scale computing resources. Station coordinates were provided by IGN. GRGS contributed to the Earth gravity field studies. In this cooperative challenge with our American colleagues, we particularly thank all the members of the Precise Orbit Determination team from GSFC (including STX), CSR, and CCAR. Their help and comments were appreciated during these long years. We thank the two reviewers for their helpful suggestions and particularly S. Klosko for his detailed remarks and fruitful advice.

References

- Antreasian, P. G., and G. W. Rosborough, Prediction of radiant energy forces on the TOPEX/POSEIDON spacecraft, *J. Spacecr. Rockets*, 29, 81–90, 1992.
- Barlier, F., C. Berger, J. Falin, G. Kockarts, and G. Thuiller, Atmospheric model based on satellite drag data, *Ann. Geophys.*, 34, 9–24, 1978.
- Berthias, J. P., C. Jayles, and D. Pradines, DIODE: A DORIS based real-time on-board orbit determination system for SPOT-4, in *Advances in the Astronautical Sciences*, vol. 84, part 1, edited by J. Teles and M. V. Samii, *Rep. AAS 93-258 1*, pp. 125–138, Am. Astron. Soc., Washington, D. C., 1993.
- Bertiger, W. I., et al., GPS precise tracking of TOPEX/POSEIDON: Results and implications, *J. Geophys. Res.*, this issue.
- Boucher, C., J.-P. Dufour, and P. Willis, The JCOD5 station coordinates solution of the DORIS network, *Tech. Rep. II*, Groupe de Rech. de Geod. Spatiale, Inst. Geogr. Natl., St. Mandé, France, June 1993.
- Christensen, E. J., et al., Calibration of TOPEX/POSEIDON at Platform Harvest, *J. Geophys. Res.*, this issue.
- Colombo, O., The dynamics of GPS and the determination of precise ephemeris, *J. Geophys. Res.*, 94, 9167–9182, 1989.
- Cretaux, J.-F., F. Nouël, C. Valorge, and P. Janniere, Introduction of empirical parameters deduced from the Hill's equations for satellite orbit determination, *Manuscr. Geod.*, 19, 135–156, 1994.
- Engelis, T., Radial orbit error reduction and sea surface topography determination using satellite altimetry, *Rep. OSU 37*, Ohio State Univ., Columbus, June 1987.
- Francis, O., and M. Bergé, Estimate of the radial orbit error by complex demodulation, *J. Geophys. Res.*, 98, 16083–16094, 1993.
- Frauenholz, R. B., T. W. Hamilton, B. E. Shapiro, and R. S. Bhat, The role of the anomalous satellite-fixed accelerations in TOPEX/POSEIDON orbit maintenance, in *AAS/AIAA Astrodynamics Specialist Conference*, Victoria, B. C., Canada, August 1993, *Rep. AAS 93-570*, Am. Astron. Soc., Washington, D. C., 1993.
- Guier, W. H., Studies on Doppler residuals, 1, Dependence on satellite orbit error and station position error, *Rep. TG-503*, Appl. Phys. Lab., Johns Hopkins Univ., Laurel, Md., June 1963.
- Kaula, W. M., *Theory of Satellite Geodesy*, Blaisdell, Waltham, Mass., 1966.
- Levine, B., *Fondements Théoriques de la Radiotechnique Statistique*, 2 vols., Mir, Moscow, 1973.
- Lucke, R. L., S. W. Sirlin, and A. M. San Martin, New definitions of pointing stability: AC and DC effects, *J. Astronaut. Sci.*, 40, 557–576, 1992.
- Marshall, J. A., S. B. Luthcke, P. G. Antreasian, and G. W. Rosborough, Modeling radiation forces acting on TOPEX/POSEIDON for precise orbit determination, *NASA Tech. Memo*, 104564, June 1992.
- McCarthy, D. D. (Ed.), IERS Standards 1992, *IERS Tech. Note 13*, Int. Earth Rotation Serv., Obs. de Paris, Nov. 1992.
- Melvin, P. J., Satellite geodesy from Orlov's plane, *Adv. Astronaut. Sci.*, 65, 1449, 1472, 1988.
- Nerem, R. S., et al., Gravity model development for TOPEX/POSEIDON: Joint gravity models 1 and 2, *J. Geophys. Res.*, this issue.
- Nouël, F., M. Deleuze, P. Laudet, and C. Valorge, Operational aspects of precise orbit determination of SPOT and TOPEX/POSEIDON satellites with DORIS, in *Advances in the Astronautical Sciences*, vol. 84, part 1, edited by J. Teles and M. V. Samii, *Rep. AAS 93-269 1*, pp. 279–290, Am. Astron. Soc., Washington, D. C., 1993.
- Rosborough, G. W., Satellite orbit perturbation due to the geopotential, *Rep. CSR-86-1*, Univ. of Tex. at Austin, Jan. 1986.
- Tapley, B. D., et al., Precision orbit determination for TOPEX/POSEIDON, *J. Geophys. Res.*, this issue.
- Wan, K.-W., J. Austin, and E. Vilar, A novel approach to the simultaneous measurement of phase and amplitude noise of oscillators, in *Proceedings of the 44th Annual Symposium on Frequency Control*, 90CH2818-3, pp. 140–144, Inst. of Electr. and Electron. Eng., New York, 1990.
- J. P. Berthias, M. Deleuze, A. Guitart, P. Laudet, F. Nouël, A. Piuze, D. Pradines, and C. Valorge, CT/TI/MS/MO, CNES bpi 1214, 18, avenue Edouard Belin, 31055 Toulouse Cedex, France. (e-mail: Internet topex@mfh.cnes.fr).
- C. Dejoie and M. F. Susini, CISI Ingénierie, 13 rue Villet, Z. I. du Palays, 31029 Toulouse, France.
- D. Taburiau, Cap Sesa Région, 8 rue Mesplé, 31036 Toulouse, France.

(Received December 2, 1993; revised April 19, 1994; accepted April 19, 1994.)